



Analysis of Vortex Flow Phenomena on Generic Delta Wing Planforms at Transonic Speeds

Andreas Hövelmann¹(✉), Andreas Winkler¹, Stephan M. Hitzel¹, Kai Richter², and Michael Werner²

¹ Airbus Defence and Space GmbH, Aerodynamic Design, Rechliner Straße, 85077 Manching, Germany

andreas.hoevelmann@airbus.com

² Deutsches Zentrum für Luft- und Raumfahrt, Institut für Aerodynamik und Strömungstechnik, Bunsenstraße 10, 37073 Göttingen, Germany

Abstract. This paper presents combined experimental and numerical investigations on the aerodynamics of a generic triple-delta wing configuration at transonic speeds up to high angles of attack with and without sideslip. Vortex flow effects such as vortex development, vortex-vortex and vortex-shock interactions are discussed for a particular wing planform, and selected results of wind tunnel tests and CFD computations are compared to each other. Thereby, a better understanding of transonic vortex flow phenomena observed is provided. The experimental analyses are based on measurements of forces and moments as well as surface pressures by pressure sensitive paint. The numerical investigations originate from URANS computations. Overall, it turns out that at low to medium angles of attack the results of both data sources are in acceptable agreement. At higher angles of attack, however, considerable discrepancies are noticed, both in the case of longitudinal and lateral motion. In particular, the experimental and numerical results emphasize a different prediction of vortex breakdown effects. These are – at the transonic conditions considered – highly linked to vortex-vortex and vortex-shock interactions.

Keywords: Vortex flow · Transonic effects · Vortex-vortex interaction · Vortex-shock interaction · Wind tunnel experiments · CFD

1 Introduction

In 2017, a German-French agreement was made on the development of a new-generation combat aircraft [1]. In this context, Airbus Defence and Space (Airbus DS, ADS) has started a feasibility study on generic and simplified low-aspect-ratio test-case models with multi-swept wing configurations, in which planform variations and their effects on the flow field are addressed. Overall, the effectiveness and sensitivity of the most driving aerodynamic shape parameters are investigated so that robust controlled flow field characteristics are provided for favored stability and control (S&C) characteristics of combat aircraft.

In total, the generic studies are based on wind tunnel (W/T) experiments and CFD simulations at sub-, trans- and supersonic conditions. The present paper focuses on the transonic regime only and presents both experimental and numerical results for a selected wing configuration at several test conditions, see Sect. 2.

In order to efficiently test and analyze such generic wing configurations and to explore the relevant design space for future combat aircraft on a simplified level, a cooperation with the German Aerospace Center (DLR) was launched, amongst others. Moreover, an international research task group was initiated by Airbus DS under the framework of the NATO-STO community, namely AVT-316 [2]. The task group called “Vortex Interaction Effects Relevant to Military Air Vehicle Performance” is active since 2018, and addresses specific research questions that are relevant to this type of multi-swept wing configurations. On the one hand, the understanding of occurring vortex flow phenomena shall thereby be enhanced. On the other hand, the capabilities of current CFD codes, including turbulence modeling, shall also be evaluated.

Overall, the wide sub- and supersonic envelope of combat aircraft requires medium- to low-aspect-ratio wing configurations, since performance and maneuverability demands often result in high angle-of-attack (AoA) conditions well beyond the attached flow regime. This also includes flight conditions with angle of sideslips (AoS) as well [3]. Moreover, this is combined with sub-, trans- and supersonic speeds and therefore significant compressibility effects. The corresponding flow fields are dominated by vortex flows and eventually, vortex-vortex and vortex-shock interactions can occur. The vortex burst behavior may dominate the longitudinal as well as the lateral stability characteristics of the aircraft, and thus the overall controllability of the vehicle [4]. Commonly, this type of wing configurations encounters instabilities such as pitch-up tendencies and roll reversals at medium to high angles of attack. This is not desirable and it is tried to shift these effects to higher angles of attack in order to extend the resulting flight envelope. Consequently, the wing planform shape has already a significant effect on the complexity of the occurring vortex flows, the associated vortex flow phenomena, and the resulting S&C characteristics. This includes the number of different leading edges, leading-edge sweep angles, additional strakes and the aspect ratio. For this reason, different types of double-delta and triple-delta wing planforms are considered and evaluated in the feasibility study of Airbus DS and the corresponding cooperation program, see Ref. [5] for additional background information.

2 The Generic Test-Case Model ADS-NA2

The wing configuration analyzed in this paper is based on the generic low-aspect-ratio test-case model ADS-NA2 that was designed by Airbus DS. It is a 1:30-scaled version of a generic combat aircraft and is equipped with different flat-plate wing planforms including sharp leading edges and sets of corresponding control surfaces. Three different wing planforms exist in total, but here, only one particular wing configuration is regarded in its zero-control variant, namely the configuration NA2_W1_SL00, see Fig. 1. It is characterized by a triple-delta wing with three different leading-edge sections. The leading-edge sweep angle of the outer main wing section is $\varphi_3 = 52.5^\circ$, while the strake section exhibits two different leading-edge sweep angles of $\varphi_1 = 52.5^\circ$

and $\varphi_2 = 75^\circ$. Further geometric details of the configuration are summarized in Table 1. For the experimental investigations, corresponding W/T models were manufactured by Airbus DS, see Sect. 3. An appropriate sting to mount the W/T model in the test section was designed and built at DLR. In the numerical investigations, see Sect. 4, the sting was also considered and included in the computations.

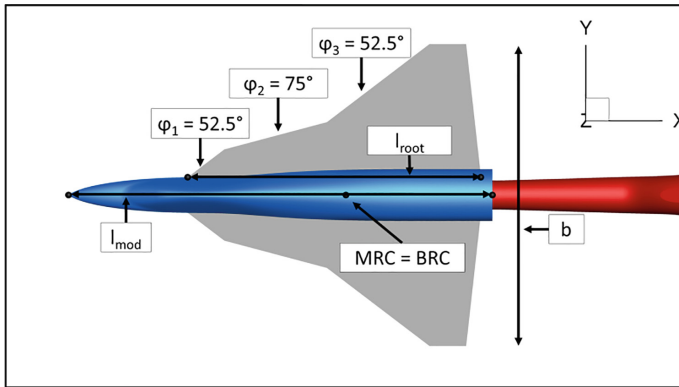


Fig. 1. ADS-NA2 test-case model – wing configuration NA2_W1_SL00.

Table 1. Geometric details of the wing configuration NA2_W1_SL00.

Model length l_{mod}	Root chord length l_{root}	Mean aerodynamic chord c_{MAC}	Wing span b	Moment reference point aft of nose x_{MRP}	Wing thickness d	Wing reference area S_{ref}
[m]	[m]	[m]	[m]	[m]	[mm]	[m ²]
0.580	0.401	0.234	0.417	0.380	8	0.082

3 Experimental Approach

The experimental investigations of the ADS-NA2 test-case model were conducted by Airbus DS and DLR as part of existing cooperation agreements in the transonic wind tunnel facilities DNW-TWG and DNW-HST of the German-Dutch Wind Tunnels in Göttingen and Amsterdam, respectively. The results shown in this paper, however, originate from the first W/T facility only [6]. The DNW-TWG is a closed circuit, continuous, sub-, trans- and supersonic wind tunnel. Of the three available and exchangeable test sections the so-called perforated test section (porosity: 6%, cross sectional area: 1 m × 1 m, length: 4.5 m) was used. With the perforated test section the wind tunnel can be operated at Mach numbers of $0.3 \leq \text{Ma} \leq 1.2$ and total pressures p_{tot} of $30 \text{ kPa} \leq p_{\text{tot}} \leq 120 \text{ kPa}$. The total temperature T_{tot} can be regulated

between $293 \text{ K} \leq T_{\text{tot}} \leq 315 \text{ K}$. The Reynolds number formed with ten percent of the square root of the cross sectional area A of the test section, $\text{Re}_{0.1\sqrt{(A)}}$, is $\text{Re}_{0.1\sqrt{(A)}} < 1.8 \times 10^6$.

Figure 2 shows the ADS-NA2 W/T model within the test section of the DNW-TWG. In the present W/T investigations, the model was installed via a rear sting on a downstream sword with integrated double-roll mechanism. In order to realize high angles of attack ($10^\circ \leq \alpha \leq 40^\circ$), an adapter with a crank angle of 15° was used together with a new rear sting that added another 10° crank angle. Angle-of-attack sweeps can be conducted either quasi-statically in a continuous sweep mode or statically in a pitch-pause mode. Due to requirements with respect to Mach number stability, however, only pitch-pause measurements were applied in the present W/T tests. The Mach number was varied between $0.5 \leq \text{Ma} \leq 1.10$ at a constant total pressure level of $p_{\text{tot}} = 95 \text{ kPa}$. The corresponding Reynolds numbers resulted in values of $\text{Re} = 7.4 \cdot 10^6$ to $\text{Re} = 13.6 \cdot 10^6$ based on a reference length of $l_{\text{Re}} = 1 \text{ m}$. Forces and moments were measured via a six-component strain gauge balance (TASK Able 1.5"). Pressure taps, temperature sensors and a dual-axis inclinometer were also integrated into the W/T model and connected to the standard instrumentation of DNW-TWG, in order to deliver required information for measurements with pressure sensitive paint (PSP) that were performed in parallel to the evaluation of forces and moments. Further information on the PSP measurement technique and its application in the present W/T investigations can be obtained from Ref. [7].

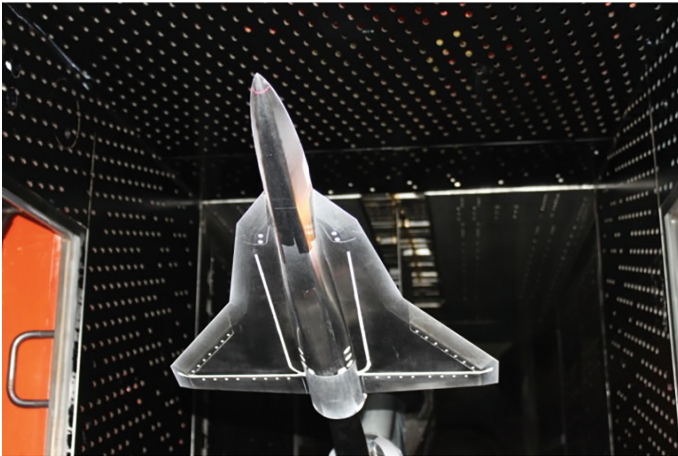


Fig. 2. ADS-NA2 W/T model within the test section of DNW-TWG, configuration NA2_W1_SL00.

4 Numerical Approach

The numerical investigations were performed with the DLR TAU code on hybrid unstructured grids. For the mesh generation process, an in-house meshing tool of Airbus DS was applied. Based on a triangulated unstructured surface grid, the boundary layer was resolved by prismatic elements close to the surfaces. In order to reach y^+ values of approximately $y^+ \approx 1$, the first cell height was set to $d_1 = 0.002$ mm and a stretching factor of $f = 1.25$ was applied. In total, 35 layers were used for the prism layer. The remaining volume was filled by tetrahedral elements. In the region of the expected vortex system, both the surface and the tetrahedral grid were considerably refined to diminish dissipation effects. The results presented below are based on a medium-sized grid with $39.0 * 10^6$ nodes for the full-wing configuration.

The CFD simulations were run as URANS computations with dual-time stepping and an implicit Backward-Euler scheme with LUSGS algorithm. The applied time step at $Ma = 0.85$ was set to $\Delta t = 4.5 * 10^{-5}$ s, which corresponds to a characteristic time step of $\Delta t^* = (\Delta t * U_\infty / c_{MAC}) \approx 0.05$. For spatial discretization, a second-order central scheme with matrix dissipation was applied. Convergence acceleration was further reached with the multigrid technique, for which a 3w cycle was used. With regard to turbulence modeling, the one-equation model SAneg with rotational correction was applied [8, 9].

5 Results

In this section, the results of the experimental and numerical investigations are presented, discussed and compared to each other. In the following, surface pressure coefficient distributions are shown for selected angles of attack and angles of sideslip, and integral aerodynamic coefficients are compared for entire angle-of-attack polars. The Mach number regarded in this analysis is $Ma = 0.85$ and the corresponding Reynolds number is $Re = 12.53 * 10^6$ based on a reference length of $l_{Re} = 1$ m.

First, the longitudinal motion with $\beta = 0^\circ$ is regarded. Figure 3 presents the surface pressure coefficient distributions of the W/T PSP and the CFD results at two angles of attack, namely $\alpha = 16^\circ$ and $\alpha = 24^\circ$. For the lower angle of attack, see Fig. 3(a) and (c), the results of both data sources are in good agreement, especially in the mid fuselage region and the front wing sections along the wing strake. Low pressure regions are noticeable close to the wing leading edges, thus showing the occurrence of leading-edge vortices. In the rear wing sections, however, differences can be observed, see for instance the outer wing region. A vortex-vortex interaction of the strake vortex and the leading-edge vortex of the outer main wing takes place. In consequence, the overall vortex system bursts and a vortex-shock interaction occurs. However, it is not obvious which effect is first and triggers the other. The shock can be observed by the distinct pressure increase and the curved pressure footprint in this region. Compared to the W/T PSP results, the chordwise position of the shock occurrence is predicted to lie further downstream in the CFD results. Moreover, the shock position in the rear fuselage region is also slightly shifted downstream.

At the higher angle of attack, see Fig. 3(b) and (d), deviations between W/T PSP and CFD results become more pronounced. Now, the overall suction levels are predicted differently over the entire triple-delta wing. In the W/T experiments, vortex bursting has moved upstream much more rapidly than in the CFD results. There, high suction levels are still present in the rear wing sections, whereas in the W/T PSP results, the rear wing sections are characterized by considerably less suction. This behavior also affects the shock position in the rear fuselage region. Compared to the experimental results, the SAneg turbulence model of the CFD computations thus attenuates the prediction of vortex breakdown effects.

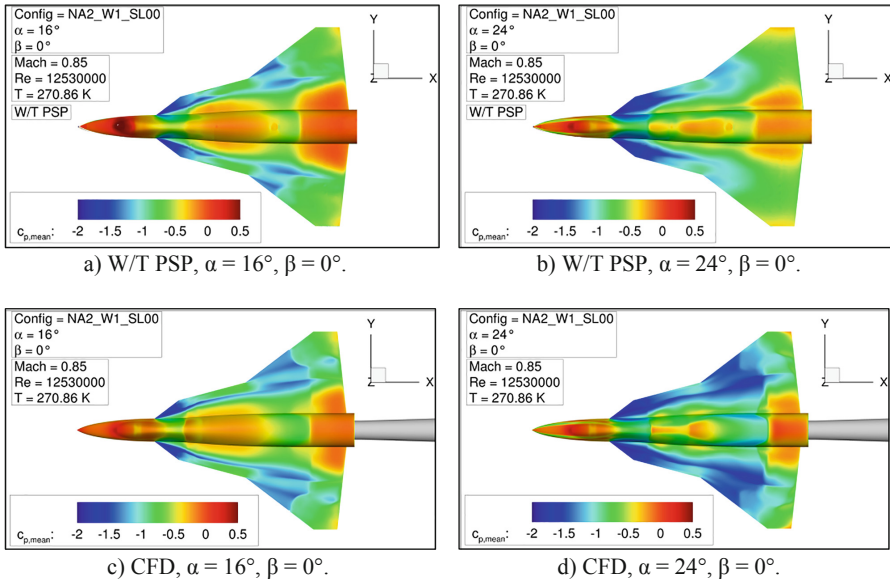


Fig. 3. Comparison of W/T PSP and CFD results – surface pressure coefficient distributions $c_{p,mean}$ at $\beta = 0^\circ$.

The corresponding aerodynamic coefficients are discussed next. Figure 4 shows the lift coefficient characteristics versus the angle of attack α at $\beta = 0^\circ$. At low to medium angles of attack ($\alpha \leq 16^\circ$) the results of W/T and CFD are in satisfactory agreement. With increasing angles of attack, however, significant deviations occur (ΔC_L up to $\approx 20\%$), which can be attributed to the characteristics of vortex breakdown discussed above. These deviations remain up to high angles of attack of $\alpha = 40^\circ$. With respect to the pitching moment coefficient characteristics, see Fig. 5, deviations in the mid to high angle-of-attack regime become even more pronounced. Pitch-up tendencies are observed in the W/T experiments at lower angles of attack than in the CFD results, which is consistent with distributions of the surface pressure coefficient discussed above. The W/T experiments further show a drop in the $C_{m,m}$ curves for $\alpha > 28^\circ$, which is not at all present in the CFD results up to $\alpha = 40^\circ$. The current results show that the agreement between W/T tests and CFD is not sufficiently satisfactory, in particular, when the pitching moment is considered.

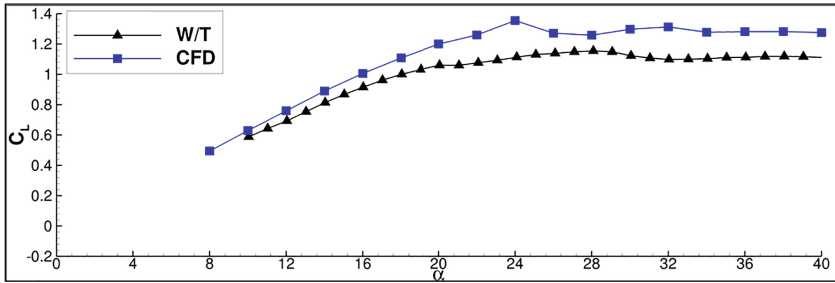


Fig. 4. Comparison of W/T and CFD results – lift coefficient C_L vs. angle of attack α at $\beta = 0^\circ$.

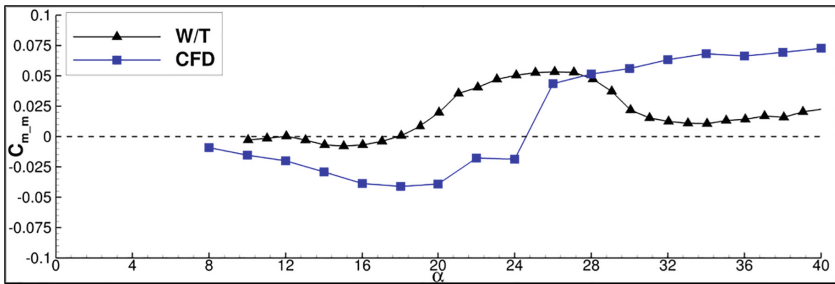


Fig. 5. Comparison of W/T and CFD results – pitching moment coefficient C_{m_m} vs. angle of attack α at $\beta = 0^\circ$.

Next, the lateral motion is regarded. Figure 6 again presents surface pressure coefficient characteristics for two different angles of attack, but now in the presence of sideslip with $\beta = 5^\circ$. For the lower angle of attack of $\alpha = 16^\circ$, see Fig. 6(a) and (c), the W/T PSP and the CFD results are in quite good agreement. Due to the positive angle of sideslip, the effective leading-edge sweep on the windward side is reduced, which leads to more intense but less stable vortices. On the leeward side, in turn, less intense but more stable vortices are expected. The asymmetric characteristics are more pronounced in the W/T PSP results than in CFD. This is noticeable in the suction regions close to the wing leading edges. In the rear fuselage region, effects of asymmetric vortices are also visible by asymmetrically occurring regions with high pressure.

At $\alpha = 24^\circ$, the surface pressure coefficient distributions of the W/T experiments and the CFD computations do not match between each other, see Fig. 6(b) and (d). Especially on the windward side, very different characteristics are noticeable. The W/T PSP results indicate that vortex bursting has propagated upstream along the entire wing so that no distinct suction levels close to the wing leading edge are present any longer. Instead, the flow field is dominated by irregular separated flow. In contrast, on the windward side the CFD results still show leading-edge suction in the front region of the wing along the strake, before vortex breakdown occurs on the outer wing. Additional W/T PSP results obtained at $\alpha = 24^\circ$ and varying angles of sideslip (not shown here) further demonstrate that the total disappearance of the windward vortex system occurs

suddenly at low angles of sideslip ($\beta \approx 2^\circ$) without any notice. On the leeward side, the agreement between W/T PSP and CFD results is better, but noticeable discrepancies are still observed. Compared to the W/T PSP results, in CFD suction levels are higher and propagate more downstream, which indicates a vortex breakdown to take place more downstream as well. Consequently, the leading-edge vortices on the leeward side are more stable in CFD than in the W/T experiments.

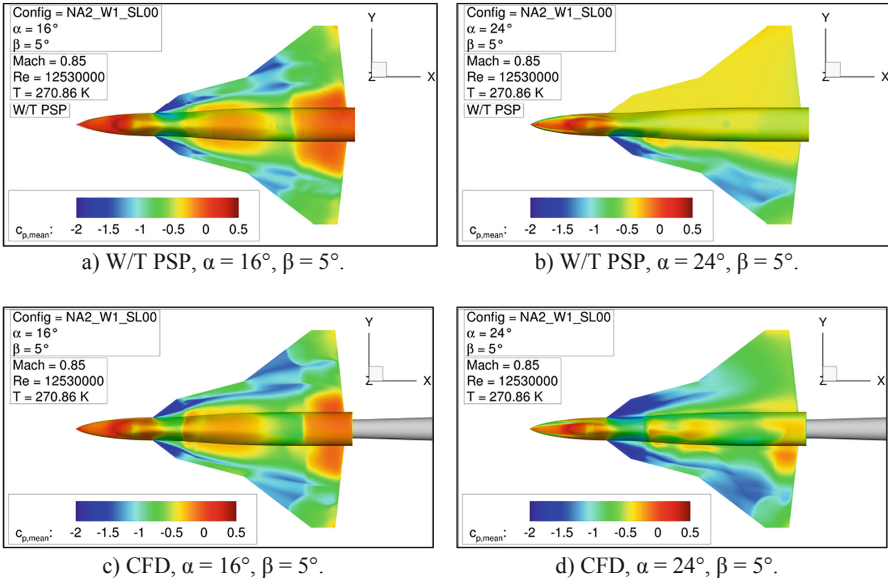


Fig. 6. Comparison of W/T PSP and CFD results – surface pressure coefficient distributions $C_{p,mean}$ at $\beta = 5^\circ$.

The resulting effects of the asymmetric surface pressure distributions on the rolling moment coefficients are displayed in Fig. 7, in which the $C_{l,m}$ values are plotted versus the angle of attack α at $\beta = 5^\circ$. This time, experimental data is only available with $\Delta\alpha = 4^\circ$. Overall, the agreement between the curves is acceptable over the entire angle-of-attack polar. With increasing angle of attack, however, noticeable differences occur, as the curves are slightly shifted. Stable characteristics with $C_{l,m} < 0$, for which the wing configuration rolls to the left and the angle of sideslip is converted to an additional angle of attack, are observed up to approximately $\alpha \approx 18^\circ$ and $\alpha \approx 20^\circ$, respectively. At higher angles of attack roll reversal then occurs because the location of vortex breakdown first moves upstream on the windward side. Thereby, the wing on the leeward side produces more lift than on the windward side. In accordance with the results of the surface pressure distributions, the roll instabilities occur earlier in the W/T experiments than in CFD. At angles of attack around $\alpha \approx 28^\circ$ to $\alpha \approx 32^\circ$, the return to stable characteristics again occurs earlier in the W/T experiments, since then vortex bursting on the leeward side also propagates upstream more rapidly as it is noticed in the CFD computations. Due to the relatively coarse resolution of the experimental

values, however, one cannot conclude that the experimental characteristics behave as smooth as the CFD predictions. Further W/T data for the considered test case, which originate from continuous sweep measurements at DNW-HST (not shown here), indicate that roll reversal occurs more suddenly and abrupt between $\alpha \approx 20^\circ$ and $\alpha \approx 24^\circ$ than it is shown in Fig. 7 by the present results. Following, the discrepancies between W/T experiments and CFD predictions tend to be higher as indicated here.

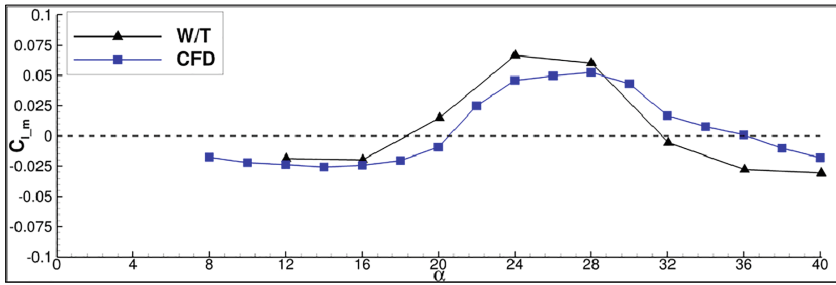


Fig. 7. Comparison of W/T and CFD results – rolling moment coefficient C_{l_m} vs. angle of attack α at $\beta = 5^\circ$.

6 Summary and Outlook

Both experimental and numerical results of the ADS-NA2 test-case model have been presented and evaluated in this paper. The analysis has focused on the aerodynamic coefficients for S&C characteristics and surface pressure coefficient distributions for flow physics effects. In the W/T experiments pressure distributions have been obtained by PSP measurements. In addition to the longitudinal motion, also the lateral motion with present sideslip has been discussed. For the considered transonic conditions, complex vortex flows occur on the generic combat aircraft. Due to the triple-delta wing configuration, a vortex system with multiple leading-edge vortices forms with increasing angle of attack. Thereby, vortex-vortex interactions take place, which entail massive vortex breakdown effects and further result in vortex-shock interactions. Consequently, the aerodynamic coefficients are highly affected, especially in the lateral motion. Pitch-up tendencies and undesired roll reversals are noticed with increasing angle of attack, which is not favored for the S&C characteristics and imply flight envelope restrictions for the generic combat aircraft.

At low to medium angles of attack ($\alpha \leq 16^\circ$), the agreement between W/T experiments and CFD computations is satisfactory. At higher angles of attack up to $\alpha = 40^\circ$, however, remarkable deviations occur in the longitudinal aerodynamic coefficients and the corresponding surface pressure distributions between both data sources. It turns out that the vortex stability and vortex breakdown effects are predicted differently in CFD, at least with the one-equation SA_{neg} turbulence model with rotation correction applied in this study. For the lateral motion with present sideslip, large deviations between experimental and numerical results are mainly observed in the surface pressure distribution with increasing angle of attack. The corresponding rolling

moment characteristics, however, still show acceptable agreement also at higher angles of attack. As an outcome of this analysis, different turbulence models are to be tested in future work for the selected test cases so that further comparisons to the existing W/T data can be made. Another way forward is the re-calibration of turbulence model parameters in the SA model, for which current research is conducted at Airbus DS and first results have recently been published [10].

Further influences of the experimental setup on the results such as the effect of wall interferences, plenum flow effects, and the effect of the actual axial pressure gradient in the W/T test section cannot be quantified for the considered transonic conditions at this stage. Specific CFD computations instead of free-flight simulations, which include the W/T test section of the DNW-TWG, would gain better knowledge in this regard. For the present study, however, this analysis was out of scope.

References

1. Factsheet Future Combat Air System – Anteil Next Generation Weapon System – NGWS. <https://www.bmvg.de/resource/blob/24288/6548107ac4b24da5611745b18252099a/20180427-factsheet-future-combat-air-system-anteil-next-generation-weapon-system-data.pdf>. Accessed October 2018
2. NATO-STO AVT-316 description. <https://www.sto.nato.int/Lists/test1/activitydetails.aspx?ID=16476>. Accessed October 2018
3. Hitzel, S.M.: Flight physical aspects and methods of future military aircraft designs. In: 63rd Deutscher Luft- und Raumfahrtkongress, Augsburg, Germany, 16–18 September 2014
4. Hitzel, S.M.: Combat aircraft vortex flow challenges – separation, interaction and breakdown. In: NATO-STO Specialists Meeting on “Progress and Challenges in Validation Testing for Computational Fluid Dynamics”, Avila, Spain, 26–28 September, no. 21 in MP-AVT-246 (2016)
5. Hitzel, S.M., Winkler, A., Hövelmann, A.: Vortex flow aerodynamic challenges in the design space for future fighter aircraft. In: STAB Symposium 2018, Darmstadt, Germany, 6–7 November 2018
6. DNW-TWG W/T information. <https://www.dnw.aero/media-center/downloads/brochures//download/3>. Accessed October 2018
7. Henne, U., Yorita, D., Klein, C.: Experimental aerodynamic high speed investigations using pressure-sensitive paint for generic delta wing planforms. In: STAB Symposium 2018, Darmstadt, Germany, 6–7 November 2018
8. Spalart, P.R., Allmaras, S.R.: A one-equation turbulence model for aerodynamic flows. In: 30th AIAA Aerospace Sciences Meeting & Exhibit, Reno (NV), United States, 6–9 January, no. 439 in AIAA (1992)
9. Allmaras, S.R., Johnson, F.T., Spalart, P.R.: Modifications and clarifications for the implementation of the Spalart-Allmaras turbulence model. In: 7th International Conference on Computational Fluid Dynamics (ICCFD7), Big Island (HI), United States, 9–13 July 2012
10. Muioli, M., Breitsamter, C., Sørensen, K.A.: Turbulence model conditioning for vortex dominated flows based on experimental results. In: 31st Congress of the International Council of the Aeronautical Sciences, Belo Horizonte, Brazil, 9–14 September, no. 4.7.2 in ICAS (2018)